



Deposited via The University of Sheffield.

White Rose Research Online URL for this paper:

<https://eprints.whiterose.ac.uk/id/eprint/225239/>

Version: Published Version

Article:

Ward, S.L., Bradley, S.L., Roseby, Z.A. et al. (2025) The role of long-term hydrodynamic evolution in the accumulation and preservation of organic carbon-rich shelf sea deposits. *Journal of Geophysical Research: Oceans*, 130 (4). e2024JC022092. ISSN: 2169-9275

<https://doi.org/10.1029/2024jc022092>

Reuse






This article is distributed under the terms of the Creative Commons Attribution (CC BY) licence. This licence allows you to distribute, remix, tweak, and build upon the work, even commercially, as long as you credit the authors for the original work. More information and the full terms of the licence here:

<https://creativecommons.org/licenses/>

Takedown

If you consider content in White Rose Research Online to be in breach of UK law, please notify us by emailing eprints@whiterose.ac.uk including the URL of the record and the reason for the withdrawal request.

The Role of Long-Term Hydrodynamic Evolution in the Accumulation and Preservation of Organic Carbon-Rich Shelf Sea Deposits

S. L. Ward¹ , S. L. Bradley² , Z. A. Roseby³ , S.-B. Wilmes¹ , D. F. Vosper³,
C. M. Roberts⁴, and J. D. Scourse³ 

¹School of Ocean Sciences, Bangor University, Wales, UK, ²School of Geography and Planning, University of Sheffield, Sheffield, UK, ³Department of Earth and Environmental Sciences, University of Exeter, Cornwall, UK, ⁴Centre for Ecology and Conservation, University of Exeter, Cornwall, UK

Key Points:

- Mapping mud and organic carbon distributions is critical for blue carbon stock assessments and effective marine management in shelf seas
- Shelf sea hydrodynamics since the Last Glacial Maximum have formed mud depocenters in the northwest European shelf
- Simulating paleoceanographic conditions improves understanding of shelf sea sediment distribution and could support blue carbon strategies

Supporting Information:

Supporting Information may be found in the online version of this article.

Correspondence to:

S. L. Ward,
sophie.ward@bangor.ac.uk

Citation:

Ward, S. L., Bradley, S. L., Roseby, Z. A., Wilmes, S.-B., Vosper, D. F., Roberts, C. M., & Scourse, J. D. (2025). The role of long-term hydrodynamic evolution in the accumulation and preservation of organic carbon-rich shelf sea deposits. *Journal of Geophysical Research: Oceans*, 130, e2024JC022092. <https://doi.org/10.1029/2024JC022092>

Received 7 NOV 2024

Accepted 14 MAR 2025

Author Contributions:

Conceptualization: S. L. Ward

Data curation: S. L. Ward, S. L. Bradley, Z. A. Roseby

Formal analysis: S. L. Ward,

S. L. Bradley, Z. A. Roseby, S.-B. Wilmes

Funding acquisition: C. M. Roberts,

J. D. Scourse

Investigation: S. L. Ward, S. L. Bradley,

J. D. Scourse

Methodology: S. L. Ward, S. L. Bradley

Resources: S. L. Ward, S. L. Bradley,

Z. A. Roseby, S.-B. Wilmes, D. F. Vosper

Supervision: J. D. Scourse

Validation: S. L. Ward

Visualization: S. L. Ward

© 2025. The Author(s).

This is an open access article under the terms of the [Creative Commons Attribution License](https://creativecommons.org/licenses/by/4.0/), which permits use,

distribution and reproduction in any medium, provided the original work is properly cited.

Abstract Understanding and mapping seabed sediment distribution in shelf seas is essential for effective coastal management, offshore developments, and for blue carbon stock assessments and conservation. Fine-grained marine sediments, particularly muds, play a key role in long-term organic carbon sequestration, so knowledge of the spatial extent of these carbon-rich deposits is important. Here, we consider how changes in shelf sea tidal dynamics since the Last Glacial Maximum have influenced the development of three mud depocenters in the northwest European shelf seas: the Fladen Ground, the Celtic Deep, and the Western Irish Sea Mud Belt. Using a new high-resolution paleotidal model, we demonstrate how the evolution of simulated tidal parameters, including bed shear stress and bottom boundary layer thickness, differ across these sites. Geological data support our findings, indicating that long-term mud sedimentation continues to the present in the Celtic Deep and Western Irish Sea Mud Belt, while in the Fladen Ground, accumulation cannot be fully explained by contemporary hydrodynamics. In the latter, mud deposition is relict, deposited during quiescent tidal conditions between 17,000 and 5,000 years ago. We suggest that simulating paleoceanographic conditions can contribute to understanding first-order sediment dynamics over large spatial and temporal scales, a key input for predictive mapping and regional blue carbon inventories. This approach is a valuable first step in data-poor regions to identify potential fine sediment deposits. By illustrating the temporal evolution of organic carbon-rich deposits, we provide a broader context for managing organic carbon storage in shelf sea sedimentary environments.

Plain Language Summary Understanding the distribution of seabed sediments is essential for managing coastal and offshore areas. Knowing where mud-rich patches are situated is particularly important in the context of the carbon cycle since shelf sea muds can store carbon over long periods. Mud deposits form due to various factors, including tidal processes, but not all result from contemporary ocean dynamics or sediment supply, with some having formed under past conditions. In this study, we examined three mud-rich areas in the northwest European shelf seas: the Fladen Ground, Celtic Deep, and Western Irish Sea Mud Belt. Using numerical ocean models to simulate postglacial ocean conditions, we found that tides influenced mud buildup differently in each of the three areas. In the Celtic Deep and Western Irish Sea Mud Belt, mud has accumulated over the past several thousands of years and continues today, especially in the latter. In the Fladen Ground, deposits are ancient relicts, preserved by calm tidal conditions since the muds have been deposited. Our research shows that modeling past ocean conditions could help map carbon-rich sediments, especially where observational data are limited. These findings are crucial for informing strategies to manage and protect organic carbon stored in seabed sediments.

1. Introduction

The understanding and prediction of shelf sea seabed sediment distributions and dynamics is critical for coastal management and planning, fisheries management, development of offshore infrastructure, marine habitat conservation, and blue carbon stock analyses. The fine-grained (mud; clay and silt) content of surficial seafloor sediments is considered the most important predictor of organic carbon content (e.g., Diesing et al., 2017, 2021; Smeaton et al., 2021; Wilson et al., 2018). These fine sediments, which often include organic-rich materials, play a key role in sequestering carbon over geological time. Here, the focus throughout is on organic carbon in the marine system, that is, carbon fixed within the tissue of living organisms during photosynthesis (Turrell et al., 2023). We use the term ‘blue carbon’ to refer to this organic carbon which is stored in the marine

Writing – original draft: S. L. Ward, S. L. Bradley, Z. A. Roseby, S.-B. Wilmes
Writing – review & editing: S. L. Ward, C. M. Roberts, J. D. Scourse

environment. In contrast, inorganic carbon in the marine system originates from calcium carbonate (e.g., from shells). Smeaton et al. (2021) illustrated that the relationship between inorganic carbon and surficial seabed sediment classification is poorly defined within the United Kingdom's Exclusive Economic Zone. However, their study demonstrated that muddy sediments store the largest quantities of organic carbon, with well-defined organic carbon hotspots identified in these areas. In most seas, organic carbon in shelf sea sediments originates from both marine sources and terrestrial inputs, such as riverine transport (Legge et al., 2020). Maintaining active deposition of organic carbon in offshore seabed sediments, as opposed to carbon stored in coastal habitats like seagrass meadows or macroalgae forests (Santos et al., 2021), requires an input of organic carbon into the system. For example, organic carbon stored in offshore sediments may originate locally from pelagic or benthic plants and animals or be transported into the area via rivers or coastal sources, subsequently advected by currents before settling in the sedimentary environment. Additionally, on the northwest European shelf seas, offshore organic carbon stores may also contain relict terrestrial carbon (de Haas et al., 2002), as large portions of the shelf were exposed during periods of lower sea levels, such as during the Last Glacial Maximum.

Effective management of blue carbon habitats and stocks, including subtidal sedimentary deposits, is important for both adapting to and mitigating the effects of climate change (Howard et al., 2023). However, designing appropriate management strategies for carbon-rich deposits requires a clear understanding of the depositional environment and the spatial extent of different seafloor sediment classes. For instance, management of relict offshore carbon-rich deposits could emphasize preservation of stored carbon, while management of active deposits could combine protection measures such as habitat restoration with strategies to enhance carbon sequestration.

The underlying mechanisms driving fine sediment accumulations in shelf seas are complex and present day hydrodynamic and morphodynamic conditions may not adequately explain surface seabed sediment distribution patterns observed across modern shelf seas. Shelf sea seabed sediments are rarely found in patches of uniform classification and so attempts to predict their spatial distribution over regional scales necessarily represents a first-order approximation. In many regions, there is a paucity of observational seabed sediment data, with significant data gaps which could be filled by synthetically predicting broad-scale sediment distribution. However, it is possible that where past shelf sea dynamics significantly differ from contemporary dynamics, simulations of past conditions may be useful for understanding sediment distribution (e.g., in the case of relict deposits). Further, since muds play a key role in predictive carbon mapping due to their capacity to store organic carbon (e.g., Diesing et al., 2017), accurately predicting the distribution of fine sediments is an important step in carbon budget assessments, especially in regions with limited data on seabed substrate or seabed organic carbon.

Williams et al. (2019) reported that extensive fine sediment (mud) deposits on the northwest European shelf seas correlated well with a predictor for tidal bottom (benthic) boundary layer (hereafter referred to as the bottom boundary layer throughout) thickness, suggesting that mud deposits exist at locations characterized by thin bottom boundary layers. This advanced previous attempts to correlate topographic and hydrodynamic variables with large-scale seabed sediment distribution (e.g., Coughlan et al., 2021; Ward et al., 2015; Wilson et al., 2018), as it extended the analysis beyond simple bed shear stresses which had limited success in predicting the spatial distribution of fine, often cohesive, sediments. However, their results were based on contemporary shelf sea hydrodynamics and could not fully explain the existence and preservation of a large relict fine-sediment deposit in the northern North Sea, the Fladen Ground. Indeed, since some fine sediment deposits are relict and so, by definition, formed under different hydrodynamic conditions, considering the temporal evolution of sediment transport parameters (e.g., tidally modulated current regimes) is crucial for understanding and predicting largescale shelf sea sediment distribution.

1.1. Development of Mud Depocenters

According to Porz et al. (2021), the development of ‘mud depocenters’ (significant areas where fine-grained terrigenous material, carbon, and contaminants accumulate on continental shelves) is driven by five key physical processes: gravity flows, oceanic fronts, resuspension by internal waves, bedload deposition under energetic flow conditions, and mud resuspension from chronic bottom trawling. While these five processes potentially combine to provide a comprehensive parametrization of mud deposition, it is not always practical to consider all of them simultaneously.

Williams et al. (2019) used sediment data alongside tidal model output to demonstrate that, in the northwest European shelf seas, regions of fine seabed sediment are located under regions of cyclonic (M_2) tidal currents. Where tidal currents rotate opposite to the Coriolis force, the bottom boundary layer thickness is reduced which serves to (a) promote deposition and inhibit resuspension of deposited fine sediments and (b) decrease the turbulence in the upper water column, which also promotes deposition of fine sediments. Williams et al. (2019) demonstrated that a predictor for bottom boundary layer thickness, incorporating tidal ellipticity (explained in detail below and sometimes referred to as tidal eccentricity), along with tidal current speed and water depth, showed reasonable spatial agreement with the distribution of seabed mud deposits on the northwest European shelf. However, this approach could not fully explain the mechanisms driving the formation of all large mud depocenters on the shelf (such as the Fladen Ground), and questions remained. Here, we explore whether these aberrant mud accumulations can be explained by considering hydrodynamic evolution over geological timescales.

1.2. Cyclonic M_2 Tidal Current Rotation and Mud Depocenters

The northwest European shelf is a tidally dominated shelf sea where offshore currents are predominantly driven by semi-diurnal tidal constituents (dominated by M_2 and S_2), along with associated nonlinear effects (Pingree & Griffiths, 1979). As the tide progresses from flood to ebb (and vice versa), tidal currents rotate clockwise or counterclockwise around pivotal points. Currents are characterized using tidal ellipses, describing their direction, semi-major and semi-minor axes lengths, and tidal phase. In the Northern Hemisphere, cyclonic tidal currents rotate counterclockwise (clockwise in the Southern Hemisphere), influencing sediment distribution patterns, as observed by Williams et al. (2019) for the northwest European shelf. Tidal ellipticity, e , can be described using the ratio of the semi-major (U_{\max}) and semi-minor (U_{\min}) components of the depth-averaged current speed:

$$e = \frac{\bar{U}_{\min}}{\bar{U}_{\max}} \quad (1)$$

where the sign of U_{\min} is negative for a clockwise rotating tidal ellipse. Therefore, in a cyclonic tidal environment in the Northern Hemisphere, where the tidal current ellipse rotates counterclockwise, the ellipticity value is positive. The degree and sign of ellipticity are relevant as they can influence the bottom boundary layer thickness in relation to the water depth, which in turn can impact on sediment transport. A relatively thin bottom boundary layer will serve to retain fine sediment deposition and promote further deposition of fines from the water column, relative to a bottom boundary layer which extends higher within the water column. Furthermore, in areas where the bottom boundary layer is thinner, a larger portion of the water column will likely have lower turbulence, compared with a more vertically homogeneous (mixed) water column. Thus, it is useful to be able to approximate the bottom boundary layer thickness over large areas, such as across an entire shelf sea, to better understand large-scale seabed sediment distribution. Using a depth-averaged tidal model of the northwest European shelf seas, Soulsby (1983) developed the following relationship to estimate the non-dimensional bottom boundary layer thickness, δ^* , at a point with depth, H :

$$\delta^* = \frac{cC_D^{1/2}}{H} \left[\bar{U}_{\max} \left(\frac{\omega - ef}{\omega^2 - f^2} \right) \right] \quad (2)$$

where ω is the radial frequency of the M_2 tide (in rad/s), f is the Coriolis parameter, $C_D = 0.0025$ (the drag coefficient), and the empirical coefficient $c = 0.075$ assigned by Soulsby (1983), based on measurements by Pingree and Griffiths (1977). For U_{\max} , see Equation 1. In shallow seas where the water depth is less than the thickness that the boundary layer would typically reach, the water column is turbulent (effectively the entire column becomes part of the bottom boundary layer, and $\delta^* \geq 1$). Where $\delta^* < 1$, the boundary layer thickness is limited by a combination of current speed, water depth, and ellipticity and is shallower than the water depth. Williams et al. (2019) showed a reasonable first-order spatial correlation between mud depocenters and 'limited bottom boundary layer thicknesses' on the northwest European shelf seas. However, unlike in other mud depocenters, across the Fladen Ground the ellipticity was not found to play a major role in suppressing the limited bottom boundary layer thickness. Indeed, the Fladen Ground is a known postglacial relict deposit (Jansen et al., 1979). Here, we explore when and under what conditions this mud depocenter accumulated.

We employ a high-resolution paleotidal model of the northwest European shelf seas, integrating the latest paleotidal boundary forcings and dynamic paleotopography. Our aims are to explore physical mechanisms driving temporal evolution of three major mud depocenters on the northwest European shelf seas since the Last Glacial Maximum and explain mud accumulations which are inconsistent with contemporary hydrodynamics. We seek to illustrate where a paleoceanographic context is needed to better understand mud depocenter development and preservation.

2. Materials and Methods

2.1. Generation of Relative Sea Level Predictions

The relative sea level and ice thickness data sets (Ward et al., 2025) required for both the global and regional tidal models were generated using a global glacial isostatic adjustment model, which solves the generalized sea level equation (Kendall et al., 2005; Mitrovica & Milne, 2003). The model includes time-dependent shoreline migration, rotation, and sea-level changes. The glacial isostatic adjustment model was solved to a maximum spherical degree of 512, which corresponds to a grid size of approximately 0.35° in latitude and longitude.

The glacial isostatic adjustment model requires an input ice sheet reconstruction which defines the spatial and temporal extent of the large continental-scale grounded ice sheets from ~ 120 ka BP (thousand years before present) to present day. We do not include floating ice shelves. For this, we followed the most recent study on glacial isostatic adjustment and relative sea level in northwest Europe (Bradley et al., 2023) and used a regional hybrid ice sheet reconstruction, combining the British-Irish, North Sea, and Eurasian ice sheet reconstructions with the North American and Antarctic ice sheet reconstructions (Bradley et al., 2016). The regional hybrid reconstruction was generated using a plastic ice sheet model (Gowan et al., 2016), incorporating the latest geomorphological and geochronological data (Clark et al., 2022). The model was run using a 1D spherically symmetrical Maxwell viscoelastic earth model with a lithosphere thickness of 71 km and an upper and lower mantle viscosity of 5×10^{20} and 5×10^{22} Pa s, respectively.

2.2. Ocean Model Forcing: Global Paleotidal Model

Global tide model simulations which were used as boundary conditions for the regional tidal model simulations were carried out with the OSU Tidal Inversion Software (OTIS) (e.g., Egbert et al., 2004; Green & Nycander, 2013; Wilmes et al., 2023) in its forward mode. OTIS solves the linearized shallow water equations (e.g., Hendershott, 1972) and allows for energy losses through bed friction and internal wave drag. Here, OTIS was used in the same setup as Wilmes et al. (2023). The simulations were carried out at $1/8^\circ \times 1/8^\circ$ horizontal resolution and were run for the tidal constituents M_2 , S_2 , K_1 , and O_1 . The model extends from 86°S to 89°N where it is bounded by an artificial vertical wall which eliminates the need for open boundary conditions. Bathymetries were based on RTOPO-2 (Schaffer et al., 2016) which was used for the present day and which incorporates GEBCO_2014 data (version 20150318, <http://www.gebco.net>). Paleobathymetry preparation followed the methodology outlined in Wilmes et al. (2023). The latest glacial isostatic model outputs for the region (see previous section) were incorporated to account for relative sea-level changes with respect to present day and were interpolated to $1/8^\circ \times 1/8^\circ$ and added to the RTOPO-2 baseline topography. Simulations were conducted from 21 ka BP to the present day (0 ka BP) at 1 ka intervals. For each 1 ka time slice, the global tidal model was configured with the corresponding paleo-conditions for that time (e.g., relative sea levels and ice sheet extent). For a detailed model validation of the present day control simulation and for further details regarding model parameterization, see Wilmes et al. (2023).

2.3. Regional Tidal Model

2.3.1. Hydrodynamic Model Set-Up

We applied TELEMAC-2D (version 8p2r0), an open-source hydrodynamic modeling system which solves the Shallow Water Equations (Saint-Venant equations) in two-dimensions (depth-averaged) (Hervouet, 2000). The hydrodynamic model was run in finite element mode, based on an unstructured triangular computational mesh grid, facilitating increased model resolution on the continental shelf and in coastal areas, with coarser resolution extending off-shelf. This unstructured grid capability maximizes the resolution of coastal processes while optimizing computational efficiency. The mesh edge lengths were set to <1.5 km in the Fladen Ground, <2 km in the

wider North Sea, 1.5–2.5 km over most of the shelf (including the Irish Sea) extending to 10–20 km at the offshore model boundaries. The entire model domain, including land, was gridded. The model was parameterized to incorporate alternate wetting and drying of coastal nodes flooded by the tide. This approach maintains all finite elements in computation, while allowing dry land and ensures mass conservation. This method was chosen for its ability to maintain a consistent computational grid across model runs, accommodating evolving coastlines and intertidal cells in response to changing relative sea levels driven by glacial isostatic adjustment and ice sheet extent. Note that the data on ice sheet thickness and extent was for grounded ice only, so there is no parameterization of floating ice in this TELEMAC model. It is the volume of grounded ice which is used in studies reconstructing past sea levels and is often referred to as the ‘ice-volume equivalent sea level’ (see Bradley et al. (2016) for further explanation) or more recently ‘barystatic sea level’ or ‘global-mean sea level’ (Gregory et al., 2019). For ease of data analysis and for subsequent use of output by others, model output was interpolated onto a structured 1/50° grid extending from –16 to 12°E and 44 to 66°N (~2.2 km in latitude and varying degree in longitude, from ~0.9 to 1.6 km).

For parameterization of friction, a constant friction coefficient of 0.035 was set in Nikuradse's law of bottom friction (Hervouet, 2000). The turbulence model with a constant viscosity coefficient was used, which represents the molecular viscosity, turbulent viscosity, and dispersion. The velocity diffusivity within this turbulence model was $1\text{e}^{-6}\text{ m}^2/\text{s}$, corresponding to the molecular viscosity of water. The internal model timestep was 20 s. Each model was run for a 30-day period, 28 days of which were output for analysis (the first two days were excluded as model spin-up), sufficient for tides-only simulations of this domain. Simulated water depth, surface elevation and u - and v components of current velocity were output at TELEMAC-2D grid nodes at hourly (instantaneous) intervals.

For consistency with Soulsby (1983), the simulated depth-averaged M_2 tidal current speeds from the regional model are used in the calculations of ellipticity, and the depth-averaged mean peak spring ($M_2 + S_2$) tidal current speed used in the estimation of the bottom boundary layer thickness.

The TELEMAC-2D model outputs the friction velocity, u_* , from which the bed shear stress (τ) was calculated:

$$\tau = \rho u_*^2 \quad (3)$$

with units N m^{-2} , where ρ is the water density ($1,025\text{ kg m}^{-3}$).

2.3.2. Model Bathymetry

The digital terrain model used was GEBCO_2023 (GEBCO Compilation Group, 2023), a global terrain model for both ocean and land (15-arc s interval grid resolution). For the present day grid, GEBCO_2023 data were mapped to the model unstructured mesh, and this was also used as the underlying bathymetric product for the paleotidal models. For each 1 ka paleo-time slice, the relative sea level (Section 2.1) was mapped to the GEBCO_2023 model bathymetry. The last step involved mapping the grounded ice sheet extent for that time slice to the paleotopography (the same ice sheet reconstructions as were used in the glacial isostatic adjustment model).

2.3.3. Regional Tidal Model Forcing

The regional tidal model, including the present day model, was forced at the boundaries using harmonic constants derived from the global tidal model (Section 2.2). Surface elevation and the u (positive eastward) and v (positive northward) components of depth-averaged tidal current velocities of the M_2 , S_2 , K_1 , and O_1 tidal constituents output from the global ocean model and available at 1 ka time slices from 21 ka BP to the present were interpolated to all boundary grid nodes. These four tidal constituents are the leading semi-diurnal and diurnal tidal constituents globally.

2.3.4. Regional Model Validation and Calibration

Comprehensive model calibration and validation were performed using tide gauge data from the northwest European shelf (Figure 1). The M_2 and S_2 tidal constituents were extracted from the model output via harmonic analysis (T_TIDE, Pawlowicz et al., 2002) and compared with harmonic constants from over 30 tide gauges in the TICON data set (Piccioni et al., 2019). Initially, model validation was conducted with model outputs driven by boundary forcing derived from the TPXO09 atlas (Egbert & Erofeeva, 2002). When compared with data from 35

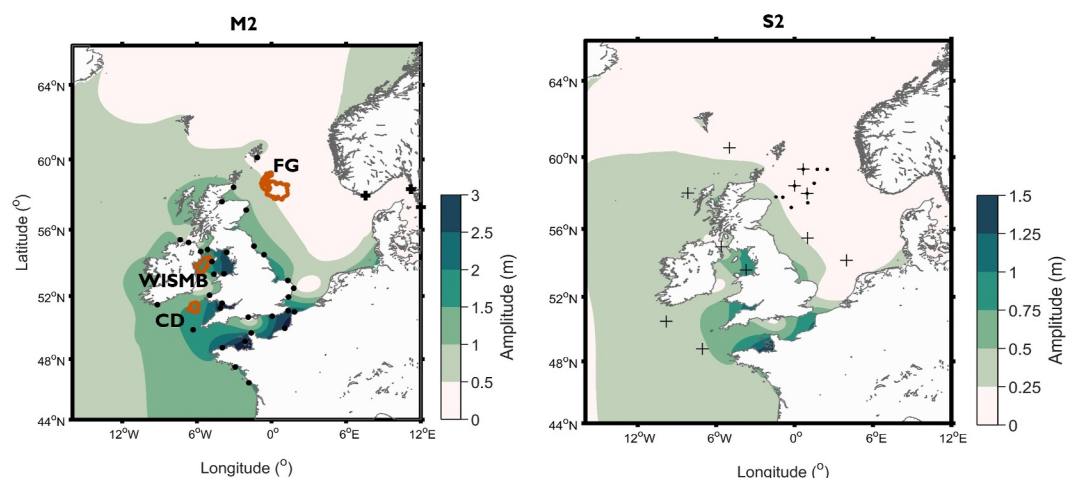


Figure 1. Simulated tidal elevation amplitudes for the dominant M_2 (left panel) and S_2 (right panel) constituents of the region. On the left panel are also the outlines of the three mud depocenters analyzed (orange polygons) where CD = Celtic Deep, WISMB = Western Irish Sea Mud Belt, FG = Fladen Ground (shown in more detail in Figure 6), and the locations of the coastal tide gauges used in the model validation, depicted by black dots and crosses (the crosses indicating those three coastal tide gauges which gave significantly poorer fit between simulated and observed S_2 constituent). On the right panel are the locations of the offshore current meter data (black dots and crosses) used in the validation of simulated tidal current speeds.

coastal tide gauges, the root mean square error (RMSE, in cm and degrees) and the scatter index (SI in percent, which is the RMSE normalized by the mean of the data) for the M_2 tidal constituent were 11 cm (7%) for elevation amplitude and 8° (4%) for phase. For the S_2 tidal constituent, validation produced 4 cm (7%) for elevation amplitude and 10° (6%) for phase.

When the TELEMAC model was forced at the boundaries using data derived from the “present day” (i.e., year 00 ka BP) global model outputs from Wilmes et al. (2023), the validation results were 12 cm (7%) and 13° (6%) for M_2 elevation amplitude and phase, respectively, and 6 cm (11%) and 64° (42%) for S_2 elevation amplitude and phase, respectively (for the same 35 coastal tide gauges). Some regional differences in the simulated S_2 tidal phases (and amplitudes, but to a lesser extent) were observed between those models forced at the boundaries by TPX009 and the global paleotidal model, which are propagated into the model domain via the boundary forcing derived from the latter. Interestingly, removing three coastal tide gauges located in the Skagerrak/Kattegat from the validation data set (thick black crosses in the left panel of Figure 1) significantly improved the S_2 validation, reducing RMSE (and SI) to 10 cm (4%) for amplitude and 6° (4%) for phase. We do not believe that this impacts on the validity of the results presented here, as the focus is on the M_2 tidal constituent and furthermore, we run validation checks of the simulated tidal currents (below). These differences are highlighted here for the benefit of those accessing our analyzed tidal model outputs.

The model's validation for tidal elevations (amplitudes and phases) was reasonable, but to ensure accuracy in velocities, observed current meter data from Guihouh et al. (2018) were used. Velocity data from seven gauges within the Fladen Ground (offshore dots on the right panel of Figure 1) were compared with simulated tidal currents, again analyzed using T_TIDE. The RMSE (and SI) for peak M_2 and S_2 tidal currents were 1.74 cm/s (7%) and 1.06 cm/s (13%), respectively. These results were based on comparisons with observed currents recorded nearest to the surface at each tide gauge (though multiple depth readings were available, they varied across sites). A second validation with a geographically dispersed subset of 11 gauges (Figure 1, crosses in the right panel) showed RMSE (and SI) values of 1.69 cm/s (5%) and 0.96 cm/s (9%), again when compared with the current meter observations from nearest the surface at each location. This comprehensive validation exercise of the present day model gave confidence in then applying the boundary forcing derived from the global paleotidal model for the paleo-time slices.

2.4. Seabed Sediment Data

Using the Seabed Substrate data set for the region from the European Marine Observation and Data Network (EMODnet), the polygons for mud and sandy mud from the Folk 7 classification were extracted. These polygons

were used to define the approximate spatial extent of the muddy sediment depocenters known as the Fladen Ground ($\sim 10,110 \text{ km}^2$), the Celtic Deep ($\sim 2,740 \text{ km}^2$), and the Western Irish Sea Mud Belt ($\sim 4,600 \text{ km}^2$) (Figures 1 and 6). To note is that the terms Witch Ground and (southern) Fladen Ground have been used interchangeably in the published literature (Böttner et al., 2019; Jansen et al., 1979; Paul & Jobson, 1991) and by public bodies such as the Joint Nature Conservation Committee (JNCC) and Center for Environment, Fisheries and Aquaculture Science (CEFAS; Eggleton et al., 2017). Here, 'Fladen Ground' refers to the entire muddy sediment body shown in Figure 1, including the Witch Ground Basin. The Fladen Ground is characterized by fine surface sediments, transitioning from muddy sands to sandy muds, to mud in the central Fladen Ground (Black et al., 2022; Johnson et al., 1993).

The focus is on these three mud depocenters because, while Williams et al. (2019) conclusively identified cyclonic M_2 tidal current rotation to be driving the reduced bottom boundary layer thickness in the Celtic Deep, their results were less definitive across the Western Irish Sea Mud Belt and the Fladen Ground. Across the Western Irish Sea Mud Belt, they suggest that the reduced bottom boundary layer thickness is driven by ellipticity at the eastern edge, while other factors, such as tidal currents or depths, influence the remainder of the mud patch. Their results for the Fladen Ground were somewhat inconclusive, indicating that additional processes may be responsible for fine sediment deposition in this region. Moreover, well-constrained geological data for each area are available in the literature (Kaskela et al., 2019; Smeaton et al., 2021) for comparison with simulated physical variables which drive sediment transport. Here, simulated physical variables (e.g., water depth, tidal current speeds) were extracted from all grid points located within these three depocenters ($\sim 2,500$, 710, 1,200 points in each of the Fladen Ground, Celtic Deep and Western Irish Sea Mud Belt, respectively) for comparison of the temporal evolution of tidally driven parameters at each mud depocenter.

3. Results

3.1. Temporal Changes in Tidal Dynamics at Three Mud Depocenters

We focus on the temporal evolution of tide-dependent parameters influencing sediment dynamics at three mud depocenters on the northwest European shelf seas since the Last Glacial Maximum. The northern North Sea was completely covered by ice at 21 ka BP. Major inundation of the North Sea occurred prior to 10 ka BP, with Dogger Bank emergent around 6–5 ka BP. The modern coastal extent of the North Sea was largely established by 6 ka BP. The Celtic Deep has remained marine throughout the entire period considered, whereas the Fladen Ground and Western Irish Sea Mud Belt were mostly inundated by 20 ka BP, and were both consistently fully submerged by 17 ka BP. Therefore, we focus our results on the period from 17 ka BP to the present day.

3.2. Relative Sea Level and Water Depth Changes

The present day water depths (mean sea level) within the three mud depocenter polygons are approximately 137 m for the Fladen Ground, 100 m for the Celtic Deep, and 80 m for the Western Irish Sea Mud Belt. Although the relative sea level histories at these depocenters show significant variation (Figure 2), particularly before 9 ka BP, the Fladen Ground has remained the deepest since all three sites became fully submerged. The rapid sea level drop which occurred across the Fladen Ground between 17 and 15 ka BP was due to localized isostatic rebound following the melting of regional ice sheets and is most pronounced at this mud depocenter due to its proximity to both the British-Irish and Fennoscandian ice sheets.

The greatest change in relative sea level in any of the three mud depocenters was in the Celtic Deep, where between 17 and 15 ka BP, mean relative sea level was approximately 66 m below contemporary sea level. As the most southern of the three depocenters, the Celtic Deep will have been most affected by the deglaciation of the other large continental ice sheets (North American ice sheet and Antarctic ice sheet) since the Last Glacial Maximum, and less so by isostatic rebound due to the unloading of regional ice sheets than the Fladen Ground and the Western Irish Sea Mud Belt (Bradley et al., 2023). Of note is that until 14 ka BP, the Celtic Deep was shallower than 50 m, which is the minimum depth threshold for offshore muddy deposits as proposed by Stephens and Diesing (2015).

The pattern of relative sea-level change across the Western Irish Sea Mud Belt was similar to that of the Fladen Ground, although at times in the past the Western Irish Sea Mud Belt was deeper than it is today. For example, at

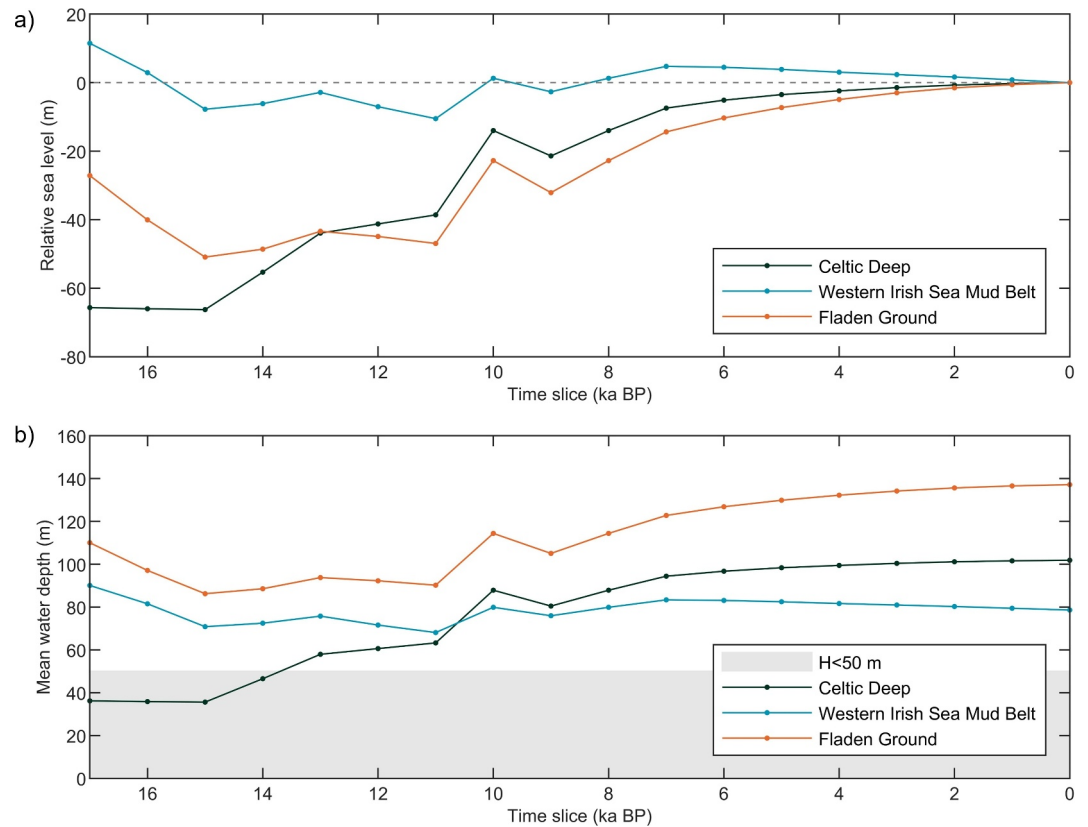


Figure 2. Temporal changes in (a) relative sea levels, referenced to present day (i.e., 0 m at 0 ka BP, dashed gray line) and (b) mean water depths across the three mud depocenters. The gray shading in the lower panel highlights water depths <50 m, which is the minimum depth threshold for offshore muddy deposits proposed by Stephens and Diesing (2015).

17 and 16 ka BP, relative sea level was 11 and 3 m above present day levels, respectively. In contrast to the other two mud depocenters, water depth in this area has decreased since 7 ka BP (from 83 to 78 m).

These variations in relative sea level histories across the Celtic Deep and the Fladen Ground will have likely played a significant role in shaping tidal dynamics and, consequently, in influencing both spatial and temporal changes in sediment transport. Given the minimal changes in water depth across the Western Irish Sea Mud Belt, other factors may have played a more significant role in driving changes in tidal dynamics at this mud depocenter.

3.3. Evolution of Tidal-Induced Bed Shear Stress

The mean present day peak bed shear stress across the three mud depocenters is consistently low (Figure 3) at approximately 0.1 N m^{-2} (Fladen Ground), 0.2 N m^{-2} (Celtic Deep) and 0.3 N m^{-2} (Western Irish Sea Mud Belt). Peak bed shear stresses in the Fladen Ground remained low throughout the simulated period, with little variation across the depocenter and with a maximum of $0.2 \pm 0.1 \text{ N m}^{-2}$ at 11 ka BP.

There has been significant temporal variation in mean peak bed shear stresses in the Celtic Deep, which were particularly high between 17 and 11 ka BP, up to a maximum of $3.5 \pm 0.6 \text{ N m}^{-2}$ at 15 ka BP, coinciding with the shallowest water at the site.

In the Western Irish Sea Mud Belt, mean peak bed shear stresses reached a maximum of $1.5 \pm 1.1 \text{ N m}^{-2}$ at 15 ka BP, corresponding to when the water depth was at one of its shallowest values. Peak bed shear stresses have been consistently low ($<0.3 \text{ N m}^{-2}$) across the Western Irish Sea Mud Belt since 10 ka BP, also with much less spatial variation across the depocenter than prior to 10 ka BP.

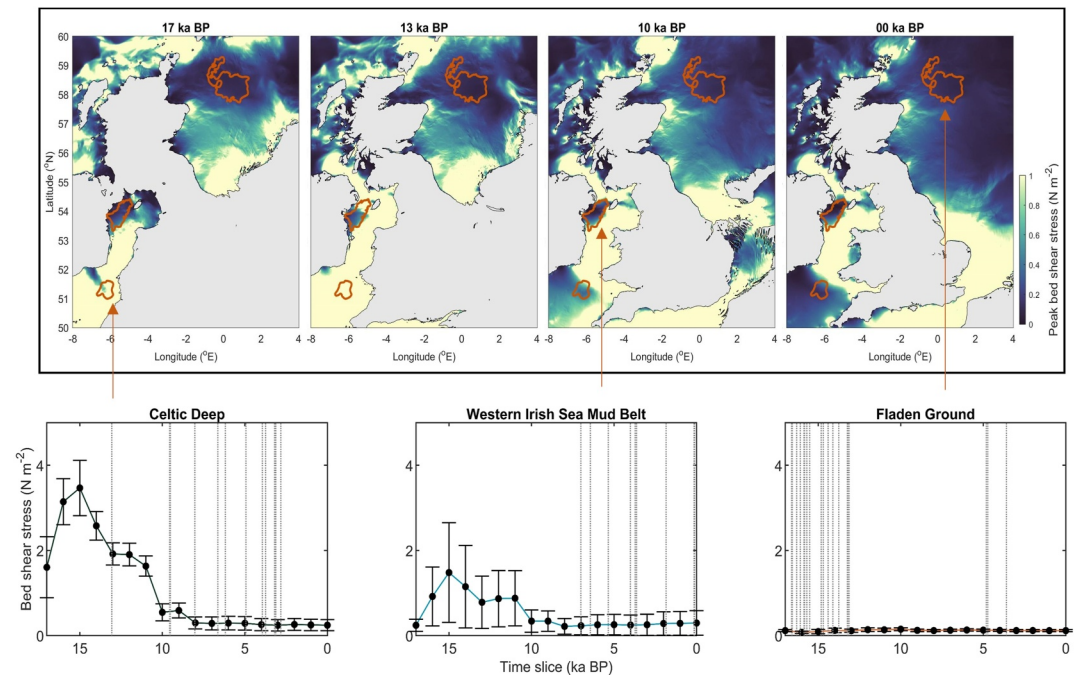


Figure 3. Top four panels: regional simulated peak bed shear stresses for selected time slices, from 17 ka BP (top left) to present day (top right, 00 ka BP). Bottom three panels: temporal evolution of simulated peak bed shear stress taken as a mean across the Celtic Deep (bottom left), Western Irish Sea Mud Belt (bottom middle), and Fladen Ground (bottom right). The solid vertical bars in each of the bottom panels illustrate one standard deviation about the mean (solid lines) and the dashed vertical lines show the calibrated radiocarbon ages of sediment samples from cores taken within each respective depocenter (see Section 4.2 for further discussion of these sediment data). Individual regional bed shear stress figures for each 1 ka time slice are available in Figure S2 in Supporting Information S1.

3.4. M_2 Tidal Current Ellipticity

The most significant regional temporal variations in ellipticity since 17 ka BP occurred in the North Sea (Figure 4). For example, depth-averaged M_2 tidal current rotation in the southern North Sea was predominantly cyclonic (positive ellipticity) around 9–8 ka BP, shortly after the inundation of this region, and this was followed by an increase in the areal extent of anticyclonic tidal current rotation in the eastern North Sea from 7 ka BP to present. Across the Fladen Ground, the mean ellipticity was positive (i.e., cyclonic) from 17 to 14 ka BP and was consistently negative (anticyclonic) from 10 ka BP onwards. This shift coincides with changes in other parameters, such as water depth, which progressively increased from 8 ka BP onwards. The Celtic Deep exhibits consistently cyclonic M_2 tidal current rotation throughout, with an ellipticity ~ 0.5 since 13 ka BP. Throughout the simulation period, the mean ellipticity over the Western Irish Sea Mud Belt remained slightly positive (cyclonic), ranging from 0 to 0.1. However, there were significant spatial variations in ellipticity across the Western Irish Sea Mud Belt, particularly between 14 and 11 ka BP (± 0.25 standard deviation), coinciding with high variability in bed shear stress across the mud depocenter.

3.5. Bottom Boundary Layer Thickness

The relative bottom boundary layer thickness is expressed as a percentage of the water column, where 100% indicates a turbulent water column in which the bottom boundary layer effectively extends throughout the water column ($\delta^* = 1$, Equation 2). Since 17 ka BP, bottom boundary layer thickness has generally decreased across the shelf (Figure 5). The present day shelf has the smallest areal extent of fully mixed water.

At no point during the period considered here has the water column over the Fladen Ground been fully mixed, with the bottom boundary layer extending to a maximum of 50% of the water column (at 12 ka BP), down to a minimum 30% in the present day. Across the Celtic Deep, on average the bottom boundary layer extended to 80% of the water column until 10 ka BP, with the water column fully mixed between 16 and 14 ka BP. There was a

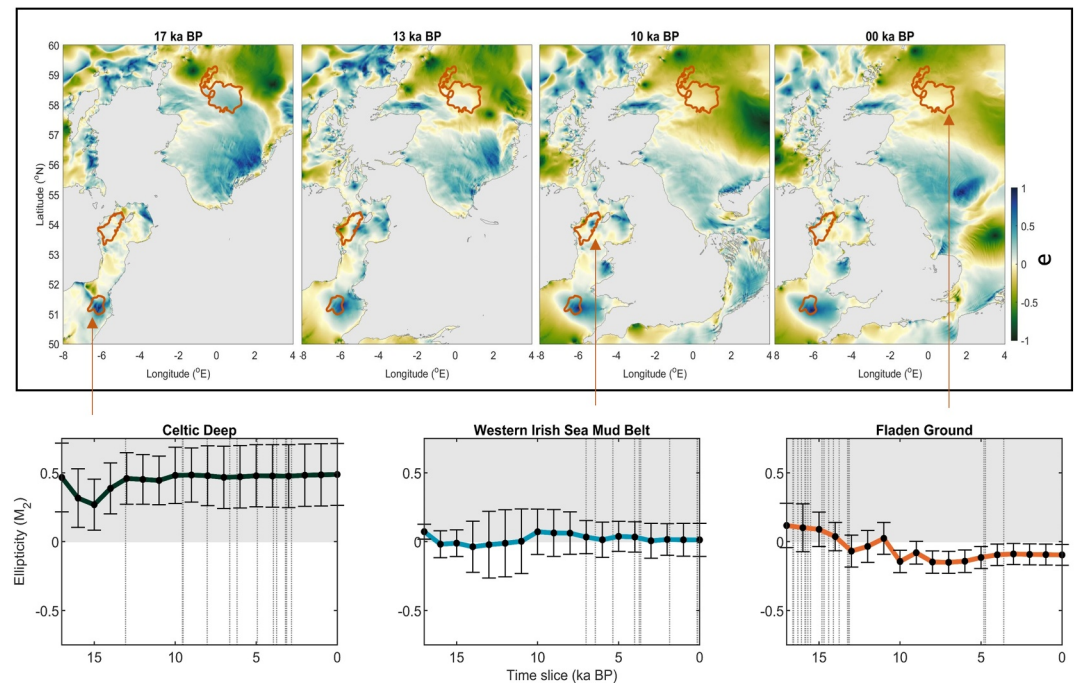


Figure 4. Top four panels: regional M_2 tidal current ellipticity for 17 ka BP (top left) through to present day (top right, 00 ka BP). Bottom three panels: temporal evolution of M_2 tidal current ellipticity at the Celtic Deep (bottom left), Western Irish Sea Mud Belt (bottom middle), and Fladen Ground (bottom right). The solid vertical bars in each of the bottom panels illustrate one standard deviation about the mean (solid lines) and the dashed vertical lines show the calibrated radiocarbon ages of sediment samples from cores taken within each respective depocenter (see Section 4.2 for further discussion of these sediment data). Where ellipticity is positive, M_2 tidal current rotation is cyclonic (counterclockwise in the Northern Hemisphere), as indicated by blue areas in the top panels. Individual figures of regional M_2 tidal current ellipticity for each 1 ka time slice are available in Figure S3 in Supporting Information S1.

significant thinning of the bottom boundary layer (from 80% to 30%) across the Celtic Deep between 11 and 10 ka BP, decreasing to a minimum 20% of the water column at the present day. Across the Western Irish Sea Mud Belt, the bottom boundary layer was relatively thin (<40%) at 17 ka BP but extended through much of the water column (>75%) from 16–11 ka BP, with a subsequent decrease (from over 80% down to ~50%) between 11 and 10 ka BP. Since 10 ka BP, the bottom boundary layer thickness across the Western Irish Sea Mud Belt has remained <55% of the water column (~50% in the present day).

3.6. The Contrasting Hydrodynamic Evolution at Three Mud Depocenters

To broadly summarize the relative temporal evolution of parameters contributing to fine sediment deposition and accumulation at each of the three mud depocenters:

- Fladen Ground: Prior to 10 ka BP, M_2 tidal current rotation was moderately cyclonic at times, but has been anticyclonic since then. Throughout the simulation period, bed shear stresses were low, and bottom boundary layer thicknesses remained less than half the water column throughout.
- Celtic Deep: Prior to 10 ka BP, the site was shallower than at present day, and shallower than 50 m from 17–15 ka BP, the limit for offshore muddy deposits (Stephens & Diesing, 2015). Furthermore, peak bed shear stresses were higher than at present, and although the M_2 tidal current rotation was cyclonic, the water column was nearly or fully mixed. From 10 ka BP to the present, water depth increased, M_2 tidal current rotation remained cyclonic, bed shear stresses decreased, and the bottom boundary layer became thinner.
- Western Irish Sea Mud Belt: Prior to 10 ka BP, water depths were ± 25 m from present day depths and the water column was fully mixed in the early Holocene. The area did not exhibit strong cyclonic tidal current rotation during the simulation period. Since 10 ka BP, bed shear stresses have been lower and the bottom

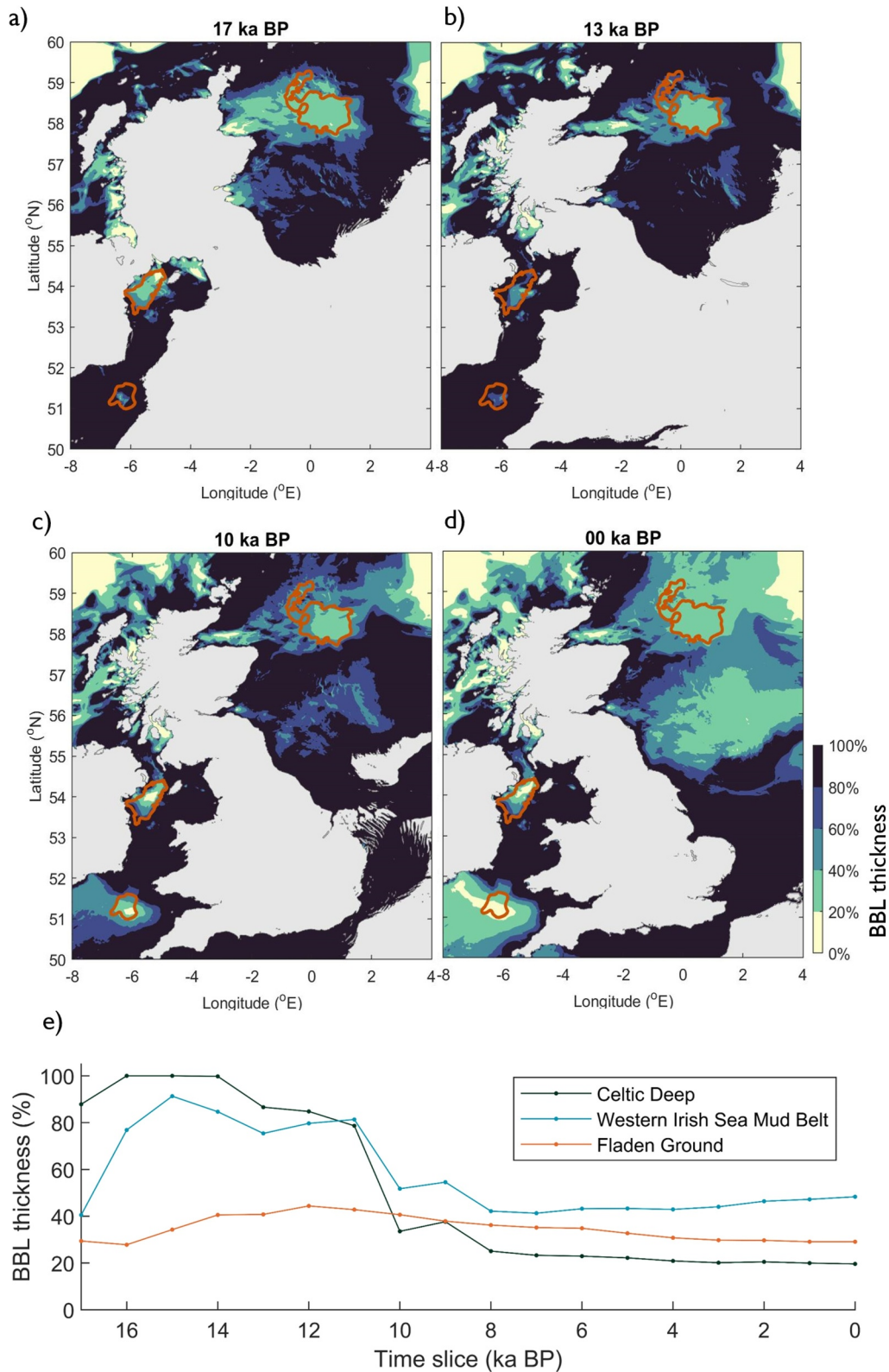


Figure 5. Panels (a–d) regional bottom boundary layer thickness for 17 ka BP (a) through to present day (d, 00 ka BP). Panel (e) temporal evolution of mean bottom boundary layer thickness across the three mud depocenters. The bottom boundary layer thickness is expressed as a percent of the water depth, where a value of 100% indicates a fully vertically mixed water column. Individual figures of regional bottom boundary layer thickness for each 1 ka time slice are available in Figure S4 in Supporting Information S1.

boundary layer thickness has been less than half of the water depth, before which it extended throughout most of the water column across much of the depocenter.

4. Discussion

4.1. Hydrodynamic Evolution at Three Mud Depocenters

Our results suggest distinct patterns in the evolution of the Fladen Ground, Celtic Deep, and the Western Irish Sea Mud Belt. The Fladen Ground has experienced a relatively quiescent tidal environment since the Last Glacial Maximum, with persistently low bed shear stresses and a thin bottom boundary layer throughout. This contrasts with the Celtic Deep and Western Irish Sea Mud Belt, which were relatively more tidally dynamic in the past, in particular prior to 10 ka BP, suggesting that the initiation of these two mud depocenters may have occurred later than at the Fladen Ground. Significant increases in bed shear stress after a period of fine sediment accumulation can lead to erosion, whereas persistently low bed shear stresses may enable relict deposits to remain.

An additional process which may have supported the retention of fine sediments in the Fladen Ground is the relatively thin bottom boundary layer, which has persisted since the region was inundated during the most recent deglaciation. A thin bottom boundary layer, often associated with fine sediment deposition, can contribute to fine sediment accumulation by suppressing near-bed turbulence (Friedrichs et al., 2000; Williams et al., 2019). Indeed, Diesing et al. (2021) concluded that the ratio of the bottom boundary layer thickness to water depth (δ^* here) was the second most important predictor variable influencing sedimentation rate in the North Sea, the most important being M_2 tidal current speed. As such, our results for relatively thicker bottom boundary layers in the Celtic Deep and Western Irish Sea Mud Belt, extending throughout much of the water column until 10 ka BP (Figure 5e) suggest that the hydrodynamic conditions at these two sites may have only become favorable for fine sediment deposition after 10 ka BP (more on this in Section 4.2). Indeed, the higher bed shear stress in the Celtic Deep during the early deglacial period would likely not have supported the deposition of fine sediments. Moreover, from 17 to 14 ka BP, the water depth in the Celtic Deep was less than 50 m, which is shallower than the 50 m minimum depth threshold for offshore muddy deposits proposed by Stephens and Diesing (2015), further supporting the narrative that this muddy deposit developed more recently than the Fladen Ground.

Williams et al. (2019) report M_2 tidal current ellipticity which is “slightly positive” (i.e., cyclonic) over the area where a “large mud deposit is present” in the northern North Sea, that is, the Fladen Ground. Our model results suggest that although mean ellipticity across the Fladen Ground was positive (i.e., cyclonic) from 17 to 14 ka BP, it was consistently negative (anticyclonic) from 10 ka BP onwards. This shift coincides with changes in other parameters, such as an increase in water depth, from 10 ka BP onwards. In contrast to Williams et al. (2019), our results indicate that present day ellipticity across the Fladen Ground is slightly negative ($e_{\text{mean}} = -0.1$, anticyclonic, clockwise rotation).

The above discrepancies in simulated ellipticity over the Fladen Ground may stem from differences in model configurations, resolution, or from the method by which the depth-averaged component of the M_2 tidal current is calculated. To explore this discrepancy, we calculated ellipticity across the Fladen Ground from the same hydrodynamic model used here (TELEMAC-2D) but forced at the model boundaries with the TPXO09 database, as per the initial model validation (see Section 2.3.4), as opposed to being forced at the model boundary using the present day global model output of Wilmes et al. (2023). This second model also generated negative mean ellipticity ($e_{\text{mean}} = -0.1$) across the modern Fladen Ground. We then calculated the ellipticity across the Fladen Ground from two other regional depth-averaged tide-only model outputs (Robins et al., 2015; Ward et al., 2016) and found them also to be consistently anticyclonic, both also with $e_{\text{mean}} \sim -0.1$. Observational current data (from ADCPs, at 53 m water depth) show anticyclonic M_2 tidal current rotation in the northern North Sea and over the Fladen Ground (Vindenes et al., 2018). Davies and Furnes (1980) also observed an anticyclonic M_2 tidal current ellipse at 36 m water depth, at one point measured within the Fladen Ground (and the same for another point at the same depth, but ~ 30 km to the east of the Fladen Ground).

Interestingly, using an early three-dimensional tidal model of the North Sea, Davies and James (1983) suggested that the M_2 tidal current ellipse in the region of the Fladen Ground rotates clockwise at the sea surface, but counterclockwise at the seabed. By way of comparison, across the Celtic Deep, all four models (the two TELEMAC-2D models and those of Robins et al., 2015; Ward et al., 2016) have strongly cyclonic conditions ($e_{\text{mean}} = +0.5$), which aligns with the results of Williams et al. (2019). The consistent finding of moderately

anticyclonic conditions across the Fladen Ground from multiple models, supported by observational data, reinforces our interpretation that the observed large sediment deposits in the region are not a product of modern hydrodynamics. Indeed, these discrepancies support the suggestion of Williams et al. (2019) that the present day ellipticity over the Fladen Ground is not driving the sediment dynamics, nor suppressing the bottom boundary layer thickness. This further highlights the importance of considering the long-term temporal evolution of physical processes which drive sediment dynamics.

4.2. Contrasting Sedimentation Rates at the Mud Depocenters

Here, we consider published sedimentation rates and age-depth models from cores taken from the three mud depocenters, to compare observed geological data with the simulated changes in hydrodynamics. Several authors have previously described Last Glacial Maximum to postglacial sediments of the Fladen Ground (Graham et al., 2010; Jansen et al., 1979; Long et al., 1986; Sejrup et al., 1994, 2009, 2014), when the area sat at the confluence of the British and Fennoscandian Ice Sheets (Graham et al., 2010). It has been noted that the rate of sediment input to the Fladen Ground decreased through the Holocene, and that, more generally, modern sedimentation across the northern and central North Sea is negligible (Figure 6; Basford & Eleftheriou, 1988; Graham et al., 2010; de Hass et al., 2002; Johnson & Elkins, 1979). Figure 6d compiles four age-depth models from sediment cores from the Fladen Ground and illustrates a low sedimentation rate after ~13 ka BP (Graham et al., 2010; Sejrup et al., 1994, 2014). Johnson and Elkins (1979) attribute this low sedimentation rate to deglaciation-induced sea-level rise, which distanced the sediment source. It is likely that the retreating grounding lines of the North Sea ice sheet (as the British-Irish- and Fennoscandian ice sheets separated) will have provided a suitable sediment source to this region in the early deglacial period and as the area became inundated, the Fladen Ground will have become increasingly distant from terrestrial sources of fine sediments. In agreement with the geological data, our model results indicate that tidally driven conditions across the Fladen Ground were favorable for fine sediment deposition during the past (e.g., low bed shear stresses, thin bottom boundary layer). The combination of these factors influencing long-term mud depocenter development highlights that an understanding of the timings and dynamics of the sediment supply is also important for interpreting fine sediment deposition.

Analysis of sediment core data from the Western Irish Sea Mud Belt by Coughlan et al. (2015) indicates that this mud depocenter remains accretionary, with the upper 0.4 m having been deposited within the last 100 years (Figure 6e). In the Western Irish Sea Mud Belt, the model results indicate high bed shear stresses before 10 ka BP and a boundary layer thickness which extended throughout most of the water column, hydrodynamic factors which likely inhibited significant fine sediment deposition. Indeed, the oldest age within the cores from this depocenter is ca. 6.4 cal kyr BP. Both the geological data and the model results align with Kershaw's (1986) findings, where sedimentation rates in seabed cores taken from the Western Irish Sea Mud Belt were minimal prior to ca. 13.7 ka BP, at 0.007 cm y^{-1} .

Sediments recovered from the Celtic Deep comprise a basal unit of coarse shelly sand and gravel, transitioning to fine silt and clay-rich muds (Austin & Scourse, 1997; Scourse et al., 2002). The observed sedimentation rate of muds in the Celtic Deep (Figure 6f) increased from the early to late Holocene, with particularly high sedimentation around ca. 6.65 cal kyr BP, when the productive frontal zone migrated over the core site (Scourse et al., 2002). These sedimentation rates align well with the model results, which suggest that tidally driven parameters such as bed shear stresses and the bottom boundary layer thickness were not conducive to significant fine sediment deposition prior to 10 ka BP. Some of the upper portion of core 51/07/199, represents an active bioturbating system and one which is also likely to be being mixed by anthropogenic disturbances such as trawling, as indicated by a ^{137}Cs profile from the core and consistent ^{14}C ages of ca. 3 cal kyr BP (Scourse et al., 2002; and Figure 6f). Scourse et al. (2002), attribute this to a slowing or cessation of sedimentation after ca. 3 cal kyr BP, with the upper 1 m of sediments consisting of relict muds, mixed with more recent organic matter through burrowing. The apparent cessation of sedimentation in the Celtic Deep, following a long-term period of increasing sedimentation rate, is interesting given the results of this study. Since 3 ka BP, across the Celtic Deep, M_2 tidal current rotation remained strongly cyclonic, and both bed shear stresses and the thickness of the bottom boundary layer remained relatively consistent (and low) and mean water depth has only increased by around 2 m (<2%). This suggests that the apparent reduction in sedimentation rate is not the result of a change in hydrodynamic conditions but could be a consequence of (a) a decrease in sediment supply or (b) removal through anthropogenic disturbance. Although beyond the remit of this study, given the importance of mud depocenters as repositories of organic carbon, future work could look to investigate the likelihood of sediment removal as the

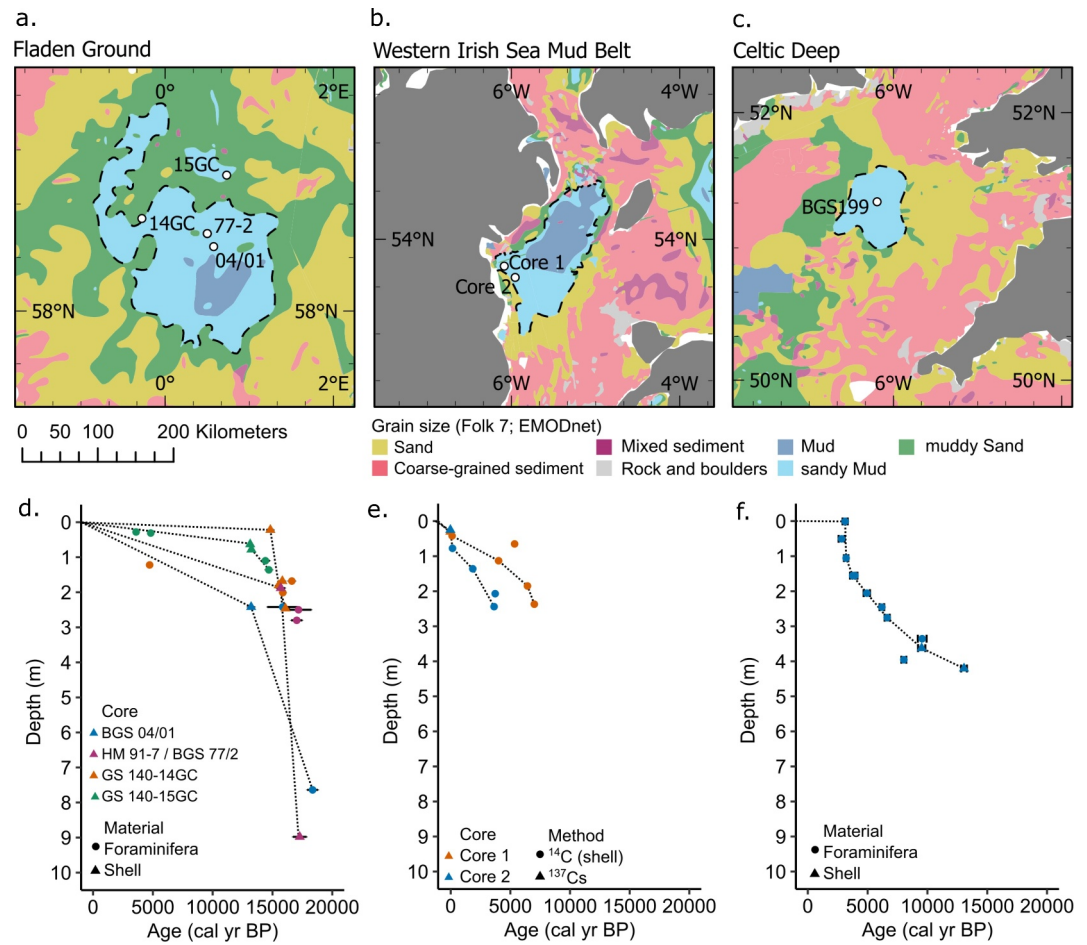


Figure 6. (a–c) Spatial distribution of sediments at the Fladen Ground, Western Irish Sea Mud Belt, and Celtic Deep, with the location of sediment cores for which age–depth models are plotted in d–f. Spatial distribution of sediments is based on a hierarchy of seven Folk classes (Folk, 1954) from EMODnet Geology. (d–f) Age–depth models for sediment cores recovered from the (d) Fladen Ground (Graham et al., 2010; Sejrup et al., 1994, 2014), (e) Western Irish Sea Mud Belt (Coughlan et al., 2015), and (f) Celtic Deep (Austin & Scourse, 1997; Scourse et al., 2002). All radiocarbon dates were recalibrated in Calib using the Marine20 calibration curve (Reimer et al., 2020). ΔR is estimated based on the average of existent proximal values, obtained from the CHRONO Marine Reservoir Database (Butler et al., 2009; Harkness, 1983; Mangerud & Gulliksen, 1975; Reimer & Reimer, 2001).

driver of the trend observed in the Celtic Deep, versus a change in the supply of fine sediments, and consider trawling as a potential mechanism.

Like most mud deposits around the United Kingdom, the Celtic Deep is intensively trawled for *Nephrops* prawns in a fishery that grew rapidly from the 1970s (Ungfors et al., 2013). Surface sediment loss due to trawling has been observed, with an estimated 20–50 cm of the upper seabed eroded in the Western Irish Sea Mud Belt (Coughlan et al., 2015), with concomitant risks of organic carbon remineralization. Porz et al. (2024) used a comprehensive modeling suite to explore the impacts of a range of trawling scenarios on sedimentary organic carbon stocks in the North Sea. Their simulations indicated high spatial variability in the impacts of trawling across different sites but overall reduced sedimentary organic carbon over a year in trawled versus untrawled simulations. The Fladen Ground, a heavily trawled and organic carbon-rich area, was highlighted as experiencing relatively high loss of organic carbon. Similarly, using modeling techniques, the results of De Borger et al. (2020) were for reduced sedimentary organic carbon content within the top 10 cm of several intensively trawled sites in the North Sea, further highlighting the potential for trawling to impact on organic carbon storage in mud depocenters.

Paleo-hydrodynamic modeling can thus provide valuable insights into the effects of human disturbance on seabed sediments, helping to differentiate whether the apparent “old” age of seafloor sediments is due to their relict nature or whether mechanical removal by resuspension and advection could be having an effect. Of course, ideally, consideration of temporal changes in sediment supply to a region would also be included, but this is not always practicable over geological timescales.

The available radiocarbon ages from the Fladen Ground sequence (Figure 6d, with associated references in the figure caption) indicate that the sediments are much older nearer the surface than at the other two mud depocenters considered here. The minimal modern sedimentation and older near-surface radiocarbon dates in the Fladen Ground suggest that it may be less effective in sequestering organic carbon today compared with more contemporary accretionary regions like the Western Irish Sea Mud Belt. As such, marine management strategies aimed at protecting and preserving seabed sediment organic carbon sequestration should focus on preserving existing sedimentary structures and habitats, rather than on the additional carbon sequestration potential of (relatively) inactive mud depocenters. Whilst mud accretion in the Fladen Ground can be explained through the hydrodynamic conditions and the supply of fine sediments, the Celtic Deep provides a third and different scenario. Given the importance of sediment supply and deposition in determining the fate of organic carbon stored in seabed sediments, this is an important avenue for future research.

Accurately estimating the sequestration capacity of blue carbon ecosystems requires understanding of fluxes of organic carbon between various marine ecosystems (Queirós et al., 2023; Santos et al., 2021). For example, this can involve the transfer of organic carbon from nearshore coastal habitats such as seagrass meadows or macroalgae forests (e.g., Krause-Jensen & Duarte, 2016; Queirós et al., 2023) to shelf sea sediments, where it may be stored over geological timescales or exported off-shelf into the deep ocean (e.g., van der Mheen, 2024). Consideration of both the biogeochemical and physical mechanisms driving this exchange is key and here we present a novel approach to understanding some of the tidally driven mechanisms, through exploring changes in shelf sea dynamics over geological timescales.

4.3. Drivers of Large-Scale Sediment Transport

While tidal processes are important for sediment dynamics over shelf seas (e.g., Pingree & Griffiths, 1979; Ward et al., 2015; Zhou et al., 2015), sediment transport and deposition results from complex interactions between processes such as sediment supply, deposition and erosion, wave effects, shelf morphology, hydrodynamics, and relative sea level. Other drivers of large-scale sediment transport over geological timescales and across continental shelves include residual circulation and sediment gravity flows (Gao & Collins, 2014, and references therein). In places, shelf sea circulation can provide pathways for fine sediment movement, and convergence of these residual currents can create regions of high fine sediment concentration (Pingree & Griffiths, 1979), while tidal resuspension may be frequent.

Over shorter timescales than those we consider here, seasonal stratification can contribute to intra-annual variations in fine sediment deposition (Wang et al., 2019); the Western Irish Sea Mud Belt, for example, is situated under a retentive seasonal gyre (Hill et al., 1994). The Fladen Ground itself is influenced by both the East Shetland Atlantic Inflow and the seasonally variable Fair Isle Current (Svendsen & Mork, 1991; Witbaard et al., 1997), which create a semi-permanent cyclonic eddy around stable, cold bottom water. Indeed, according to Basford and Eleftheriou (1988), the Fair Isle Current significantly affects the composition, grain size, and organic carbon content of sediments in the northern and central North Sea. This interplay of hydrodynamic factors and sediment characteristics justifies further exploration to fully understand their impacts on sediment dynamics and carbon sequestration in the region.

Comprehensive modeling of the processes driving sediment transport over shelf sea scales is a complex task. In this study, we focused on the simpler first-order relationship between tidal-induced ellipticity, bed shear stress, bottom boundary layer thickness, and known mud depocenters on the northwest European shelf, as established by Williams et al. (2019), and based on work by Soulsby (1983). Future work on incorporating more sediment-driving processes into these modeling studies would be valuable, in particular wave-induced sediment transport. The spatial and temporal evolution of wave-induced bed shear stresses is also important over geological timescales (Neill et al., 2009, 2010).

Hanebuth et al. (2015) explored the temporal evolution of mud depocenters in continental shelf seas, suggesting that their initiation is controlled by local environmental conditions. According to Hanebuth et al. (2015), mud belts often form around nuclei determined by seafloor morphology rather than sediment sources. They propose two methods for dating the onset of deposition: (a) radiocarbon dating of core samples from the base of the depocenter and (b) using acoustic data to establish stratigraphy combined with sea-level curves. We propose a third method through paleotidal modeling, as demonstrated here. This approach serves as a valuable first step in data-poor regions to identify potential fine sediment deposits likely to have been accumulating for some time, prior to embarking on more expensive offshore data collection and radiocarbon dating.

Advancing blue carbon stock assessments requires further efforts in mapping sedimentary basins, sampling sediment cores, and evaluating carbon burial rates. So far, predictions of fine sediment accumulations and organic carbon distribution across shelf seas have focused on modern shelf dynamics (e.g., DIESING et al., 2021; EPSTEIN et al., 2024; WILSON et al., 2018), whereas our findings highlight the critical role of past tidal conditions in the formation of mud depocenters like the Fladen Ground, where deposition is relict. Integrating both historical and contemporary physical processes offers a more comprehensive foundation for accurately quantifying the long-term carbon storage potential of shelf sea environments.

5. Conclusions

Using a new regional paleotidal model alongside existing geological data, we illustrate the contrasting evolution of hydrodynamic variables across three major mud depocenters on the northwest European shelf seas. In the Celtic Deep, geological data indicate most mud accumulation has occurred in the past ~10 ka, with earlier tidal conditions too energetic for fine sediment deposition. Similarly, in the Western Irish Sea Mud Belt, simulations suggest more quiescent tidal conditions from ~10 ka BP onwards, supported by geological data indicating significant fine sediment accumulation there from ~7 ka BP onward. The Fladen Ground, a known relict deposit, appears to have been consistently tidally quiescent since the region was fully submerged at around 17 ka BP, allowing the fine sediments which accumulated there until ~5 ka BP to remain. Our findings highlight the importance of millennial scale hydrodynamic evolution in preserving fine, often carbon-rich, sediment deposits. While paleotidal models can enhance our understanding of sedimentary depositional environments, most predictive seabed substrate maps focus on modern hydrodynamics and so lack the temporal dimension needed to capture a comprehensive history of basin evolution. This is especially relevant to efforts seeking to understand sediment dynamics, fine sediment deposits and hence the stability of carbon-rich deposits in data-poor regions. As such, we conclude that the approach demonstrated here should be an important step for accurately assessing and managing long-term organic carbon storage in shelf sea environments as blue carbon.

Data Availability Statement

The full suite of analyzed tidal model output, analysis scripts, glacial isostatic model output (relative sea level and ice sheet extent data sets), as well as the geological data are available at Zenodo via [10.5281/zenodo.14795629](https://doi.org/10.5281/zenodo.14795629) with Creative Commons Attribution 4.0 International (Ward et al., 2025). Figures 1–5 were made with MATLAB Version: 9.11.0.1769968 (R2021b; The MathWorks Inc, 2021). Figure 6 was made with RStudio version 2.023.03.0 + 368 (RStudio Team, 2023) and Inkscape version 1.2.2 (Inkscape Project, 2022).

References

- Austin, W. E. N., & Scourse, J. D. (1997). Evolution of seasonal stratification in the Celtic sea during the Holocene. *Journal of the Geological Society*, *154*(2), 249–256. <https://doi.org/10.1144/gsjgs.154.2.0249>
- Basford, D., & Eleftheriou, A. (1988). The benthic environment of the North Sea (56° to 61°N). *Journal of the Marine Biological Association of the United Kingdom*, *68*(1), 125–141. <https://doi.org/10.1017/s0025315400050141>
- Black, K. E., Smeaton, C., Turrell, W. R., & Austin, W. E. N. (2022). Assessing the potential vulnerability of sedimentary carbon stores to bottom trawling disturbance within the UK EEZ. *Frontiers in Marine Science*, *9*. <https://doi.org/10.3389/fmars.2022.892892>
- Böttner, C., Berndt, C., Reinardy, B. T. I., Geersen, J., Karstens, J., Bull, J. M., et al. (2019). Pockmarks in the Witch ground basin, central North Sea. *Geochemistry, Geophysics, Geosystems*, *20*(4), 1698–1719. <https://doi.org/10.1029/2018gc008068>
- Bradley, S. L., Ely, J. C., Clark, C. D., Edwards, R. J., & Shennan, I. (2023). Reconstruction of the palaeo-sea level of Britain and Ireland arising from empirical constraints of ice extent: Implications for regional sea level forecasts and North American ice sheet volume. *Journal of Quaternary Science*, *38*(6), 791–805. <https://doi.org/10.1002/jqs.3523>
- Bradley, S. L., Milne, G. A., Horton, B. P., & Zong, Y. (2016). Modelling sea level data from China and Malay-Thailand to estimate Holocene ice-volume equivalent sea level change. *Quaternary Science Reviews*, *137*, 54–68. <https://doi.org/10.1016/j.quascirev.2016.02.002>

Acknowledgments

The authors acknowledge funding from Convex Group Ltd for the Convex Seascape Survey, which is facilitated by Blue Marine Foundation (www.bluemarinefoundation.com/projects/convex-seascape-survey). The model simulations (of both SLW and SBW) were conducted on Supercomputing Wales, a collaboration between Welsh universities and the Welsh Government. The authors are grateful for ongoing technical support from Dr Ade Fewings and team (Digital Services, Bangor University). SBW was funded by The Leverhulme Trust, Research Grant RPG-2021-091 and NERC Grant NE/S009566/1. SLW would like to thank Professors Alan G. Davies, Mattias Green, and Peter Robins for many shelf-sea related discussions. We are grateful to the two reviewers and to the journal editor for their constructive comments and careful review of our manuscript.

- Butler, P. G., Scourse, J. D., Richardson, C. A., Wanamaker Jr, A. D., Bryant, C. L., & Bennell, J. D. (2009). Continuous marine radiocarbon reservoir calibration and the ^{13}C Suess effect in the Irish Sea: Results from the first multi-centennial shell-based marine master chronology. *Earth and Planetary Science Letters*, 279(3–4), 230–241. <https://doi.org/10.1016/j.epsl.2008.12.043>
- Clark, C. D., Ely, J. C., Hindmarsh, R. C. A., Bradley, S., Ignéczi, A., Fabel, D., et al. (2022). Growth and retreat of the last British–Irish ice sheet, 31 000 to 15 000 years ago: The BRITICE-CHRONO reconstruction. *Boreas*, 51(4), 699–758. <https://doi.org/10.1111/bor.12594>
- Coughlan, M., Guerrini, M., Creane, S., O'Shea, M., Ward, S. L., Van Landeghem, K. J., et al. (2021). A new seabed mobility index for the Irish Sea: Modelling seabed shear stress and classifying sediment mobilisation to help predict erosion, deposition, and sediment distribution. *Continental Shelf Research*, 229, 104574. <https://doi.org/10.1016/j.csr.2021.104574>
- Coughlan, M., Wheeler, A. J., Dorschel, B., Lordan, C., Boer, W., Van Gaever, P., et al. (2015). Record of anthropogenic impact on the Western Irish Sea mud belt. *Anthropocene*, 9, 56–69. <https://doi.org/10.1016/j.ancene.2015.06.001>
- Davies, A. M., & Furnes, G. K. (1980). Observed and computed M2 tidal currents in the North Sea. *Journal of Physical Oceanography*, 10(2), 237–257. [https://doi.org/10.1175/1520-0485\(1980\)010%3C0237:OACMTC%3E2.0.CO;2](https://doi.org/10.1175/1520-0485(1980)010%3C0237:OACMTC%3E2.0.CO;2)
- Davies, A. M., & James, I. D. (1983). Three-dimensional Galerkin-Spectral sea models of the North Sea and German bight. *North Sea Dynamics*, 85, 85–94. https://doi.org/10.1007/978-3-642-68838-6_5
- De Borger, E., Tiano, J., Braeckman, U., Rijnsdorp, A. D., & Soetaert, K. (2020). Impact of bottom trawling on sediment biogeochemistry: A modelling approach. *Biogeosciences Discussions*, 2020(8), 1–32. <https://doi.org/10.5194/bg-18-2539-2021>
- de Haas, H., van Weering, T. C., & de Stigter, H. (2002). Organic carbon in shelf seas: Sinks or sources, processes and products. *Continental Shelf Research*, 22(5), 691–717. [https://doi.org/10.1016/S0278-4343\(01\)00093-0](https://doi.org/10.1016/S0278-4343(01)00093-0)
- Diesing, M., Kröger, S., Parker, R., Jenkins, C., Mason, C., & Weston, K. (2017). Predicting the standing stock of organic carbon in surface sediments of the North–West European continental shelf. *Biogeochemistry*, 135(1–2), 183–200. <https://doi.org/10.1007/s10533-017-0310-4>
- Diesing, M., Thorsnes, T., & Bjarnadóttir, L. R. (2021). Organic carbon densities and accumulation rates in surface sediments of the North Sea and Skagerrak. *Biogeosciences*, 18(6), 2139–2160. <https://doi.org/10.5194/bg-18-2139-2021>
- Egbert, G. D., & Erofeeva, S. Y. (2002). Efficient inverse modeling of barotropic ocean tides. *Journal of Atmospheric and Oceanic Technology*, 19(2), 183–204. [https://doi.org/10.1175/1520-0426\(2002\)019%3C0183:EIMOB0%3E2.0.CO;2](https://doi.org/10.1175/1520-0426(2002)019%3C0183:EIMOB0%3E2.0.CO;2)
- Egbert, G. D., Ray, R. D., & Bills, B. G. (2004). Numerical modeling of the global semidiurnal tide in the present day and in the last glacial maximum. *Journal of Geophysical Research*, 109(C3). <https://doi.org/10.1029/2003JC001973>
- Eggleton, J., Murray, J., McIlwaine, P., Mason, C., Noble-James, T., Hinchey, H., et al. (2017). JNCC/Cefas partnership report series.
- Epstein, G., Fuller, S. D., Hingmire, D., Myers, P. G., Peña, A., Pennelly, C., & Baum, J. K. (2024). Predictive mapping of organic carbon stocks in surficial sediments of the Canadian continental margin. *Earth System Science Data*, 16(5), 2165–2195. <https://doi.org/10.5194/essd-16-2165-2024>
- Folk, R. L. (1954). The distinction between grain size and mineral composition in sedimentary-rock nomenclature. *The Journal of Geology*, 62(4), 344–359. <https://doi.org/10.1086/626171>
- Friedrichs, C. T., Wright, L. D., Hepworth, D. A., & Kim, S. C. (2000). Bottom-boundary-layer processes associated with fine sediment accumulation in coastal seas and bays. *Continental Shelf Research*, 20(7), 807–841. [https://doi.org/10.1016/S0278-4343\(00\)00003-0](https://doi.org/10.1016/S0278-4343(00)00003-0)
- Gao, S., & Collins, M. B. (2014). Holocene sedimentary systems on continental shelves. *Marine Geology*, 352, 268–294. <https://doi.org/10.1016/j.margeo.2014.03.021>
- GEBCO Compilation Group (2023). GEBCO 2023 grid. <https://doi.org/10.5285/f98b053b-0cbe-6c23-e053-6c86abc0af7b>
- Gowan, E. J., Tregoning, P., Purcell, A., Lea, J., Fransner, O. J., Noormets, R., & Dowdeswell, J. A. (2016). ICESHEET 1.0: A program to produce paleo-ice sheet reconstructions with minimal assumptions. *Geoscientific Model Development*, 9(5), 1673–1682. <https://doi.org/10.5194/gmd-9-1673-2016>
- Graham, A. G. C., Lonergan, L., & Stoker, M. S. (2010). Depositional environments and chronology of Late Weichselian glaciation and deglaciation in the central North Sea. *Boreas*, 39(3), 471–491. <https://doi.org/10.1111/j.1502-3885.2010.00144.x>
- Green, J. A. M., & Nycander, J. (2013). A comparison of internal wavedrag parameterizations for tidal models. *Journal of Physical Oceanography*, 43(1), 104–119. <https://doi.org/10.1175/JPO-D-12-023.1>
- Gregory, J. M., Griffies, S. M., Hughes, C. W., Lowe, J. A., Church, J. A., Fukumori, I., et al. (2019). Concepts and terminology for sea level: Mean, variability and change, both local and global. *Surveys in Geophysics*, 40(6), 1251–1289. <https://doi.org/10.1007/s10712-019-09525-z>
- Guihou, K., Polton, J., Harle, J., Wakelin, S., O'Dea, E., & Holt, J. (2018). Kilometric scale modeling of the North West European Shelf Seas: Exploring the spatial and temporal variability of internal tides. *Journal of Geophysical Research: Oceans*, 123(1), 688–707. <https://doi.org/10.1002/2017jc012960>
- Hanebuth, T. J. J., Lantsch, H., & Nizou, J. (2015). Mud depocenters on continental shelves—Appearance, initiation times, and growth dynamics. *Geo-Marine Letters*, 35(6), 487–503. <https://doi.org/10.1007/s00367-015-0422-6>
- Harkness, D. D. (1983). The extent of natural ^{14}C deficiency in the coastal environment of the United Kingdom. *Proceedings of the First International Symposium 14 C and Archaeology, Groningen, 1981*(8), 351–364.
- Hendershott, M. C. (1972). Numerical models of ocean tides. *Sea*, 6, 47–95.
- Hervouet, J. M. (2000). TELEMAC modelling system: An overview. *Hydrological Processes*, 14(13), 2209–2210. [https://doi.org/10.1002/1099-1085\(200009\)14:13<3.CO;2-Y](https://doi.org/10.1002/1099-1085(200009)14:13<3.CO;2-Y)
- Hill, A. E., Durazo, R., & Smeed, D. A. (1994). Observations of a cyclonic gyre in the western Irish Sea. *Continental Shelf Research*, 14(5), 479–490. [https://doi.org/10.1016/0278-4343\(94\)90099-X](https://doi.org/10.1016/0278-4343(94)90099-X)
- Howard, J., Sutton-Grier, A. E., Smart, L. S., Lopes, C. C., Hamilton, J., Kleypas, J., et al. (2023). Blue carbon pathways for climate mitigation: Known, emerging and unlikely. *Marine Policy*, 156, 105788. <https://doi.org/10.1016/j.marpol.2023.105788>
- Inkscape Project. (2022). Inkscape. Retrieved from <https://inkscape.org>
- Jansen, J. H. F., Doppert, J. W. C., Hoogendoorn-Toering, K., de Jong, J., & Spaink, G. (1979). Late pleistocene and Holocene deposits in the Witch and Fladen ground area, northern North Sea. *Netherlands Journal of Sea Research*, 13(1), 1–39. [https://doi.org/10.1016/0077-7579\(79\)90031-0](https://doi.org/10.1016/0077-7579(79)90031-0)
- Johnson, H., Richards, P. C., Long, D., & Graham, C. C. (1993). *United Kingdom offshore regional report: The geology of the northern North Sea*. HMSO for the British Geological Survey. (British Geological Survey.)
- Johnson, T. C., & Elkins, S. R. (1979). Holocene deposits of the Northern North Sea: Evidence for dynamic control of their mineral and chemical composition. *Geologie en Mijnbouw*, 58(3), 353–366.
- Kaskela, A. M., Kotilainen, A. T., Alanen, U., Cooper, R., Green, S., Guinan, J., et al. (2019). Picking up the pieces—Harmonising and collating seabed substrate data for European maritime areas. *Geosciences*, 9(2), 84. <https://doi.org/10.3390/geosciences9020084>
- Kendall, R. A., Mitrovica, J. X., & Milne, G. A. (2005). On post-glacial sea level – II. Numerical formulation and comparative results on spherically symmetric models. *Geophysical Journal International*, 161(3), 679–706. <https://doi.org/10.1111/j.1365-246X.2005.02553.x>

- Kershaw, P. J. (1986). Radiocarbon dating of Irish Sea sediments. *Estuarine, Coastal and Shelf Science*, 23(3), 295–303. [https://doi.org/10.1016/0272-7714\(86\)90029-6](https://doi.org/10.1016/0272-7714(86)90029-6)
- Krause-Jensen, D., & Duarte, C. M. (2016). Substantial role of macroalgae in marine carbon sequestration. *Nature Geoscience*, 9(10), 737–742. <https://doi.org/10.1038/ngeo2790>
- Legge, O., Johnson, M., Hicks, N., Jickells, T., Diesing, M., Aldridge, J., et al. (2020). Carbon on the northwest European shelf: Contemporary budget and future influences. *Frontiers in Marine Science*, 7, 143. <https://doi.org/10.3389/fmars.2020.00143>
- Long, D., Bent, A., Harland, R., Gregory, D. M., Graham, D. K., & Morton, A. C. (1986). Late quaternary palaeontology, sedimentology and geochemistry of a vibrocore from the Witch ground basin, central North Sea. *Marine Geology*, 73(1–2), 109–123. [https://doi.org/10.1016/0025-3227\(86\)90114-3](https://doi.org/10.1016/0025-3227(86)90114-3)
- Mangerud, J., & Gulliksen, S. (1975). Apparent radiocarbon ages of recent marine shells from Norway, Spitsbergen, and Arctic Canada. *Quaternary Research*, 5(2), 263–273. [https://doi.org/10.1016/0033-5894\(75\)90028-9](https://doi.org/10.1016/0033-5894(75)90028-9)
- Mitrovica, J. X., & Milne, G. A. (2003). On post-glacial sea level: I. General theory. *Geophysical Journal International*, 154(2), 253–267. <https://doi.org/10.1046/j.1365-246X.2003.01942.x>
- Neill, S. P., Scourse, J. D., Bigg, G. R., & Uehara, K. (2009). Changes in wave climate over the northwest European shelf seas during the last 12,000 years. *Journal of Geophysical Research*, 114(C6). <https://doi.org/10.1029/2009JC005288>
- Neill, S. P., Scourse, J. D., & Uehara, K. (2010). Evolution of bed shear stress distribution over the northwest European shelf seas during the last 12,000 years. *Ocean Dynamics*, 60(5), 1139–1156. <https://doi.org/10.1007/s10236-010-0313-3>
- Paul, M. A., & Jobson, L. M. (1991). Geotechnical properties of soft clays from the Witch ground basin, central North Sea. *Engineering Geology - Special Publication*, 7(1), 151–156. <https://doi.org/10.1144/gsl.eng.1991.007.01>
- Pawlowicz, R., Beardsley, R. C., & Lentz, S. J. (2002). Classical tidal harmonic analysis including error estimates in MATLAB. *Ocean Modelling*, 5(3), 371–380. [https://doi.org/10.1016/S1463-5003\(02\)00003-8](https://doi.org/10.1016/S1463-5003(02)00003-8)
- Piccioni, G., Dettmering, D., Bosch, W., & Seitz, F. (2019). Ticon: Tidal CONstants based on GESLA sea-level records from globally located tide gauges. *Geoscience Data Journal*, 6(2), 97–104. <https://doi.org/10.1002/gdj3.72>
- Pingree, R. D., & Griffiths, D. K. (1977). The bottom mixed layer on the continental shelf. *Estuarine and Coastal Marine Science*, 5(3), 399–413. [https://doi.org/10.1016/0302-3524\(77\)90064-0](https://doi.org/10.1016/0302-3524(77)90064-0)
- Pingree, R. D., & Griffiths, D. K. (1979). Sand transport paths around the British Isles resulting from M2 and M4 tidal interactions. *Journal of the Marine Biological Association of the United Kingdom*, 59(2), 497–513. <https://doi.org/10.1017/S0025315400042806>
- Porz, L., Zhang, W., Christiansen, N., Kossack, J., Daewel, U., & Schrum, C. (2024). Quantification and mitigation of bottom-trawling impacts on sedimentary organic carbon stocks in the North Sea. *Biogeosciences*, 21(10), 2547–2570. <https://doi.org/10.5194/bg-21-2547-2024>
- Porz, L., Zhang, W., Hanebuth, T. J., & Schrum, C. (2021). Physical processes controlling mud depocenter development on continental shelves—geological, oceanographic, and modeling concepts. *Marine Geology*, 432, 106402. <https://doi.org/10.1016/j.margeo.2020.106402>
- Queirós, A. M., Tait, K., Clark, J. R., Bedington, M., Pascoe, C., Torres, R., et al. (2023). Identifying and protecting macroalgae detritus sinks toward climate change mitigation. *Ecological Applications*, 33(3), e2798. <https://doi.org/10.1002/eap.2798>
- Reimer, P. J., Austin, W. E., Bard, E., Bayliss, A., Blackwell, P. G., Ramsey, C. B., et al. (2020). The IntCal20 Northern Hemisphere radiocarbon age calibration curve (0–55 cal kBP). *Radiocarbon*, 62(4), 725–757. <https://doi.org/10.1017/RDC.2020.41>
- Reimer, P. J., & Reimer, R. W. (2001). A marine reservoir correction database and on-line interface. *Radiocarbon*, 43(2A), 461–463. <https://doi.org/10.1017/S003822200038339>
- Robins, P. E., Neill, S. P., Lewis, M. J., & Ward, S. L. (2015). Characterising the spatial and temporal variability of the tidal-stream energy resource over the northwest European shelf seas. *Applied Energy*, 147, 510–522. <https://doi.org/10.1016/j.apenergy.2015.03.045>
- RStudio Team. (2023). *RStudio*. Integrated Development for R. RStudio, PBC. Retrieved from <http://www.rstudio.com/>
- Santos, I. R., Burdige, D. J., Jennerjahn, T. C., Bouillon, S., Cabral, A., Serrano, O., et al. (2021). The renaissance of Odum's outwelling hypothesis in Blue Carbon science. *Estuarine, Coastal and Shelf Science*, 255, 107361. <https://doi.org/10.1016/j.ecss.2021.107361>
- Schaffer, J., Timmermann, R., Arndt, J. E., Kristensen, S. S., Mayer, C., Morlighem, M., & Steinhage, D. (2016). A global, high-resolution data set of ice sheet topography, cavity geometry, and ocean bathymetry. *Earth System Science Data*, 8(2), 543–557. <https://doi.org/10.5194/essd-8-543-2016>
- Scourse, J. D., Austin, W. E. N., Long, B. T., Assinder, D. J., & Huws, D. (2002). Holocene evolution of seasonal stratification in the Celtic sea: Refined age model, mixing depths and foraminiferal stratigraphy. *Marine Geology*, 191(3–4), 119–145. [https://doi.org/10.1016/S0025-3227\(02\)00528-5](https://doi.org/10.1016/S0025-3227(02)00528-5)
- Sejrup, H. P., Hafliðason, H., Aarseth, I., King, E., Forseberg, C. F., Long, D., & Rokoengen, K. (1994). Late Weichselian glaciation history of the northern North Sea. *Boreas*, 23, 1–13. <https://doi.org/10.1111/j.1502-3885.1994.tb00581.x>
- Sejrup, H. P., Hjelstuen, B. O., Nygård, A., Hafliðason, H., & Mardal, I. (2014). Late Devensian ice-marginal features in the central North Sea—Processes and chronology. *Boreas*, 44, 1–13. <https://doi.org/10.1111/bor.12090>
- Sejrup, H. P., Nygård, A., Hall, A. M., & Hafliðason, H. (2009). Middle and late Weichselian (Devensian) glaciation history of south-western Norway, North Sea and eastern UK. *Quaternary Science Reviews*, 28(3–4), 370–380. <https://doi.org/10.1016/j.quascirev.2008.10.019>
- Smeaton, C., Hunt, C. A., Turrell, W. R., & Austin, W. E. (2021). Marine sedimentary carbon stocks of the United Kingdom's exclusive economic zone. *Frontiers in Earth Science*, 9, 593324. <https://doi.org/10.3389/feart.2021.593324>
- Soulsby, R. L. (1983). *The bottom boundary layer of shelf seas* (Vol. 35, pp. 189–266). Elsevier oceanography series. [https://doi.org/10.1016/S0422-9894\(08\)70503-8](https://doi.org/10.1016/S0422-9894(08)70503-8)
- Stephens, D., & Diesing, M. (2015). Towards quantitative spatial models of seabed sediment composition. *PLoS One*, 10(11), e0142502. <https://doi.org/10.1371/journal.pone.0142502>
- Svendsen, E., & Mork, M. (1991). Features of the northern North Sea circulation. *Continental Shelf Research*, 11(5), 493–508. [https://doi.org/10.1016/0278-4343\(91\)90055-B](https://doi.org/10.1016/0278-4343(91)90055-B)
- The MathWorks Inc. (2021). *MATLAB version: 9.11.0.1769968 (R2021b)*. The MathWorks Inc. Retrieved from <https://www.mathworks.com>
- Turrell, W. R., Austin, W. E. N., Philbrick, S. P., Tilbrook, C., & Kennedy, H. (2023). Clarifying the role of inorganic carbon in blue carbon policy and practice. *Marine Policy*, 157, 105873. <https://doi.org/10.1016/j.marpol.2023.105873>
- Ungfors, A., Bell, E., Johnson, M. L., Cowing, D., Dobson, N. C., Bublit, R., & Sandell, J. (2013). Nephrops fisheries in European waters. *Advances in Marine Biology*, 64, 247–314. <https://doi.org/10.1016/B978-0-12-410466-2.00007-8>
- van der Mheen, M., Wernberg, T., Pattiaratchi, C., Pessarrodona, A., Janekovic, I., Simpkins, T., et al. (2024). Substantial kelp detritus exported beyond the continental shelf by dense shelf water transport. *Scientific Reports*, 14(1), 839. <https://doi.org/10.1038/s41598-023-51003-5>
- Vindenes, H., Orvik, K. A., Søiland, H., & Wehde, H. (2018). Analysis of tidal currents in the North Sea from shipboard acoustic Doppler current profiler data. *Continental Shelf Research*, 162, 1–12. <https://doi.org/10.1016/j.csr.2018.04.001>

- Wang, A., Ralston, D. K., Bi, N., Cheng, Z., Wu, X., & Wang, H. (2019). Seasonal variation in sediment transport and deposition on a muddy clinoform in the Yellow Sea. *Continental Shelf Research*, *179*, 37–51. <https://doi.org/10.1016/j.csr.2019.04.009>
- Ward, S., Bradley, S., & Roseby, Z. (2025). Dataset: The role of long-term hydrodynamic evolution in the accumulation and preservation of organic carbon-rich deposits in the shelf seas. *Zenodo*. [Dataset]. <https://doi.org/10.5281/zenodo.14795629>
- Ward, S. L., Neill, S. P., Scourse, J. D., Bradley, S. L., & Uehara, K. (2016). Sensitivity of palaeotidal models of the northwest European shelf seas to glacial isostatic adjustment since the Last Glacial Maximum. *Quaternary Science Reviews*, *151*, 198–211. <https://doi.org/10.1016/j.quascirev.2016.08.034>
- Ward, S. L., Neill, S. P., Van Landeghem, K. J., & Scourse, J. D. (2015). Classifying seabed sediment type using simulated tidal-induced bed shear stress. *Marine Geology*, *367*, 94–104. <https://doi.org/10.1016/j.margeo.2015.05.010>
- Williams, M. E., Amoudry, L. O., Brown, J. M., & Thompson, C. E. L. (2019). Fine particle retention and deposition in regions of cyclonic tidal current rotation. *Marine Geology*, *410*, 122–134. <https://doi.org/10.1016/j.margeo.2019.01.006>
- Wilmes, S. B., Pedersen, V. K., Schindelegger, M., & Green, J. A. M. (2023). Late Pleistocene evolution of tides and tidal dissipation. *Paleoceanography and Paleoclimatology*, *38*(11), e2023PA004727. <https://doi.org/10.1029/2023PA004727>
- Wilson, R. J., Speirs, D. C., Sabatino, A., & Heath, M. R. (2018). A synthetic map of the north-west European Shelf sedimentary environment for applications in marine science. *Earth System Science Data*, *10*(1), 109–130. <https://doi.org/10.15129/1e27b806-1eae-494d-83b5-a5f4792c46fc>
- Witbaard, R., Duineveld, G. C. A., & De Wilde, P. A. W. J. (1997). A long-term growth record derived from Arctica Islandica (Mollusca, Bivalvia) from the Fladen ground (northern North Sea). *Journal of the Marine Biological Association of the United Kingdom*, *77*(3), 801–816. <https://doi.org/10.1017/S0025315400036201>
- Zhou, C., Dong, P., & Li, G. (2015). Hydrodynamic processes and their impacts on the mud deposit in the Southern Yellow Sea. *Marine Geology*, *360*, 1–16. <https://doi.org/10.1016/j.margeo.2014.11.012>